Available online at www.sciencedirect.com
SCIENCE DIRECT®
Journal of Solid State Chemistry 177 (2004) 2818–2826
JOURNAL OF SOLID STATE CHEMISTRY
http://elsevier.com/locate/jssc

Preparation and characterization of intercalated misfit-layer compounds and natural superlattices

Y. Ohno* and S. Shimokawa

Department of Electrical and Electronic Engineering, Faculty of Engineering, Utsunomiya University, 7-1-2 Yoto, Utsunomiya 321-8585, Tochigi, Japan

Received 3 December 2003; received in revised form 28 January 2004; accepted 4 April 2004

Abstract

This paper presents the preparation and characterization of the new types of misfit-layer compounds and natural superlattices consisting of $Ce_xNb_{1-x-y}\square_yS$ (Q′) and Ni_zNbS_2 (H) layers, where $\square$ is an atomic deficit at a metal site. A Q′ layer is larger by about 1 Å in thickness than a CeS (Q) layer in $(CeS)_{1.16}NbS_2$. They are prepared by chemical vapor transport reaction in a closed silica tube under quasi-equilibrium conditions. The 1Q′/3H type of compound are grown as a single crystal while the 1Q′/4H type of compound is grown as composite crystals with the 1Q′/3H and 1Q/2H compounds. Natural superlattices which have a long period in a direction perpendicular to layers are found. Their chemical formulae are given by $(Ce_xNb_{1-x-y}\square_yS)_m(Ni_z)_{n-m}(NbS_2)_n$, where m and n are integers. It is found from an X-ray-photoelectron spectroscopy (XPS) study that Nb affects the valence and the bonding of Ce in the Q′ layers. It is in a higher oxidation state than Nb in NbS_2 layers. A scanning tunneling microscope (STM) study shows that some of the superlattices form a hexagonal $\sqrt{3}a_0 \times \sqrt{3}a_0R30^\circ$ supercell in the (a,b)-plane and behave as a narrow-gap semiconductor so that no STM images are obtained at bias voltage less than 0.3 eV.

Keywords: Misfit-layer compounds; Natural superlattices; Intercalation

1. Introduction

Recently, a great interest has been taken in multilayer materials of layer thickness less than 10 nm because they exhibit exotic properties such as quantum electron localization, giant magnetic resistivity and high-temperature superconductivity. The mQ/nH type of misfit-layer compounds which are represented by the chemical formula $\{(MX)_{1+x}\}_m(TX_2)_n$ (M = Sn, Sb, Pb, Bi and rare-earth elements; T = Ti, V, Cr, Nb and Ta; X=S and Se) have been studied extensively since 1985 when the unique crystal structure was reported by Diaz et al. [1–3].

The 1Q/1H compounds are constructed by alternately stacking a MX (Q) layer with pseudo-quadratic symmetry and a TX_2 (H) layer with slightly distorted hexagonal symmetry. Both layers are incommensurate along the a-axis. They are regarded as intercalation derivatives of layered transition-metal dichalcogenides (LTMDCs) in a broad sense because both materials have many similar characters such as charge transfer to a TX_2 layer, the easy preparation of higher-stage complexes and minor changes in the electronic structure of a pristine TX_2 layer. Charge transfer to a TX_2 layer was confirmed for rare-earth misfit-layer compounds more than a decade ago. However, for misfit-layer compounds containing Pb and Sn it has been controversial for a long time. Recently, the angle-resolved photoelectron spectroscopy studies, combined with the density functional calculations have shown that the conduction band of the H layers in $(PbS)_{1.14}TS_2$ (T = Ti and Nb) and $(SnS)_{1.20}NbS_2$ is filled with additional electrons transferred from PbS or SnS layers [4–6]. The electronic structure of a pristine TS_2 layer changes a little in forming the misfit-layer compounds. Main variations are the shift of the Fermi level, the opening of a $p-d$ gap and the reduced width of a S 3p-derived band. Similar variations were found in the alkali–metal intercalation derivatives of TiS_2, which were attributed

*Corresponding author. Fax: +81-28-649-5236.
E-mail address: ohno@cc.utsunomiya-u.ac.jp (Y. Ohno).

0022-4596/$ - see front matter © 2004 Elsevier Inc. All rights reserved.
doi:10.1016/j.jssc.2004.04.007

to charge transfer effects and the more ionic character of a Ti–S bond [7,8]. In spite of the variations, the electronic structure is understood by superposition of the energy bands of each constituent layer and the rigid-band model has been applied to the photoelectron spectra, the X-ray absorption spectra and the electron energy-loss spectra [9–11]. Till now the 1Q/1H, 1Q/2H, 1Q/3H, 1Q/4H, 1.5Q/1H and 2Q/1H types of misfit-layer compounds have been discovered [2–14]. It has been found that transferred electrons per H layer decrease with the number of layers sandwiched by two successive Q layers [15]. A similar phenominon happens in the stage complexes of alkali–metal–intercalated graphite [16]. Thus we may regard the 1Q/1H, 1Q/2H, 1Q/3H, 1Q/4H types of misfit-layer compounds as stage-1, stage-2, stage-3 and stage-4 compounds of LTMDCs, respectively.

They are also regarded as one-dimensional natural superlattices with a short period of a few nanometers. In the compounds different types of layers are regularly stacked on the atomic scale without losing their inherent character. Bulk and surface plasmons of these compounds have been treated, using the superlattice theory of Camley and Mills [17,18]. The unique feature of these compounds is to have definite interfaces easily cleaved with adhesive tape.

This paper presents the preparation and characterization of the new types of lamellar misfit-layer compounds containing $Ce_xNb_{1-x}\square_yS$ (Q′) and $Ni_z(NbS_2)_2$ (H) layers, where $\square$ is an atomic deficit at a metal site and $x\sim0.6$ and $y\sim0.1$. The 1Q′/3H compound is found as a single crystal while the 1Q′/4H compound is discovered in the form of a composite crystal. The term 'composite crystal' used here means that a crystal is made up of more than two different crystal parts, which are accompanied with crystal imperfections introduced by stacking faults and plural screw dislocations. Higher-stage compounds are also grown in the same silica tube, which form a supercell along the *c*-axis. The *c* lattice constant is a few hundred Å.

2. Experiments

The crystals of $(Ce_xNb_{1-x-y}\square_yS)(Ni_z)_2(NbS_2)_3$, $(Ce_xNb_{1-x-y}\square_yS)(Ni_z)_3(NbS_2)_4$ and $(Ce_xNb_{1-x-y}\square_yS)_m(Ni_z)_{n-m}(NbS_2)_n$ ($n>10$) were grown by chemical vapor transport reaction from the mixture of Ni, Nb, Ce_2S_3 and S in the atomic ratio of 0.6:4:1:7. The mixture was contained in an evacuated and then sealed silica tube of inner diameter of 15 mm and length of about 300 mm. A small amount of iodine is employed as a transport reagent. A silica tube was placed in a two-zone electric furnace. The mixture was heated to 880°C gradually to avoid the explosion of the silica tube. During crystal growth, the high and low temperature zones of the furnace were kept at 960°C and 880°C, respectively. Lamellar crystals were grown in the high and intermediate temperature zones after reaction for three weeks.

Grown crystals were analyzed by means of X-ray diffraction (XRD), X-ray fluorescence (XRF) and X-ray photoelectron spectroscopy (XPS) methods. XRD measurements were made in the 2θ range of 6–80° with monochromatized Cu$K\alpha_1$ radiation ($\lambda=1.54056$ Å). The scanning rate of a goniometer was 4°/min and a chart speed was 20 and 80 mm/min. The crystals were classified from XRD patterns into several groups. Chemical compositions were investigated by the point XRF analysis which was suitable for small samples and local analyses of the area of about 1 mm ∅, using the Rigaku XRF instrument (model ZSK 100e). The Ce 3*d*, Ni 2*p* and Nb 3*d* XPS spectra were measured with a commercially available X-ray generator equipped with Mg and Al dual anodes and a double-pass cylindrical-mirror-analyzer (CMA). The operation conditions of an X-ray tube were 15 kV and 20 mA. Scanning tunneling microscope (STM) images were obtained in the constant current mode at room temperature. Atomically ordered images were taken at a tunneling current less than 1 nA and bias voltage of ~0.7 V, using a mechanically polished Pt–Ir tip. Atomically clean and smooth surfaces were prepared by a cleavage in the atmosphere just before the measurements. STM observations and XPS measurements were performed on cleaved surfaces under ultra-high vacuum (UHV) conditions.

3. XRD results

The XRD patterns of grown crystals and a powder left after the reaction are shown in Fig. 1. They reveal only intensive (00*l*) lines. The *c* lattice constant of a remaining powder has been estimated to be 17.40 Å. This value is nearly equal to the sum of the thicknesses of a CeS layer and a Ni_zNbS_2 layer, i.e., $5.47+11.88=17.35$ Å [3,19]. As the thickness of the $(NbS_2)_2$ layer remains almost unchanged with Ni uptake [19], the powder may be identified as $Ni_z(CeS)_{1.16}(NbS_2)_2$, the Ni-intercalated derivative of the 1Q/2H misfit-layer compound. In the same ampoule the crystals of new misfit-layer compounds of the 1Q′/3H and 1Q′/4H types are grown. They are represented by $(Ce_xNb_{1-x-y}\square_yS)(Ni_z)_{n-1}(NbS_2)_n$ ($n=3$ and 4). The 1Q′/3H compound is grown as a single crystal. The c lattice constant is 24.33 Å, which is larger by about 1 Å as compared with the total thickness of a CeS layer and a triple Ni_zNbS_2 layer, i.e., $5.47+5.94\times3=23.29$ Å. Its difference reduces to the lattice expansion of the Q′ layer. Meerschaut and co-worker [20,21] have found the commensurate needle-shaped crystals of $(Nb_{1-x}La_xS)(NbS_2)_n$ ($n=1$ and 2; $x\sim0.3$). In the crystals $Nb_{1-x}La_xS$

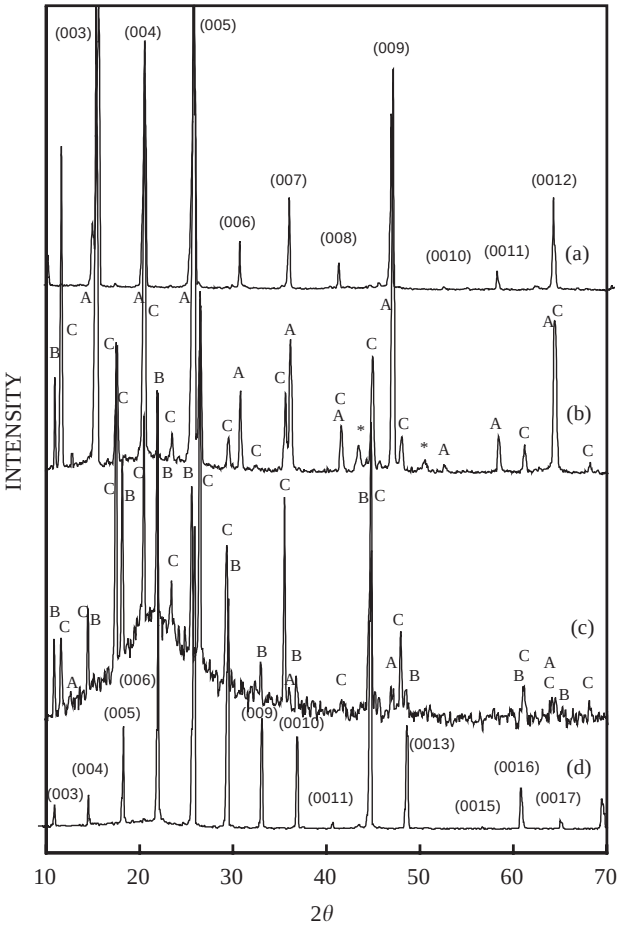

Fig. 1. XRD patterns of grown crystals and a powder left after reaction in a silica tube. (a) Powder sample of $Ni_z(CeS)_{1.16}(NbS_2)_2$, which belongs to the 1Q/2H type of compound. (b) Sample 1 and (c) sample 2 are composite crystals consisting of 1Q/2H, 1Q′/3H and 1Q′/4H compounds. (d) Single crystal of the 1Q′/3H compound. Notations A, B and C represent a diffraction line from 1Q/2H, 1Q′/3H and 1Q′/4H compounds, respectively. Asterisk marks show a diffraction line from a steel holder. The XRD pattern of the sample 2 shows a broad peak centered at $2\theta = 22°$, which is caused by diffuse X-ray scattering from a glass holder.

layer is rotated by 45° in the (a, b)-plane with respect to NbS_2 layers and the lattice extends along the c-axis by about 0.5 Å as compared with a LaS layer in $(LaS)_{1.14}NbS_2$. The XRD patterns in Fig. 1 show that the sample 1 is a composite crystal of the 1Q/2H, 1Q′/3H and 1Q′/4H types of compounds and dominant parts are made up of the 1Q/2H and 1Q′/4H compounds. The c lattice constant of the 1Q′/4H compound is 30.35 Å, in near agreement with the total thickness of a Q′ layer and a quadruple H layer, i.e., $6.51 + 5.94 \times 4 = 30.27$ Å. The sample 2 is also a composite crystal with 1Q/2H, 1Q′/3H and 1Q′/4H compounds, although the dominant parts are the 1Q′/3H and 1Q′/4H compounds. No crystals are found for the 1Q′/1H and 1Q′/2H compounds. This fact implies that the Q′ layers are stable in higher-stage complexes. It is very interesting crystallographically in relation to charge transfer and the creation of a large supercell.

Many fine diffraction lines which arise from a superlattice are often observed. They are shown in Figs. 2 and 3. As the sample 4 contains a crystal part of $Ni_z(CeS)_{1.16}(NbS_2)_2$, fine diffraction lines are superimposed on the intensive lines of the 1Q/2H compound and from the sublattice of Ni_zNbS_2. Their intervals are nearly equal in a range between the (002) and (004) lines of Ni_zNbS_2. Then the c lattice constants (c_s) of the samples 3, 4 and 5 are estimated from the number of the lines in the limited range and the c lattice constant of Ni_zNbS_2 to be about 260, 155 and 185 Å, respectively. Provided that the superlattices are constructed of layers of about 6 Å, the c lattice constants correspond to about 43, 26 and 31 layers, respectively. The atomic composition of a superlattice is Ni (0.31):Ce (0.07):Nb(1.00):S (2.20) for the sample 4. Then the chemical formula is written by $(Ce_{0.56}Nb_{0.32}\square_{0.12}S)_3(Ni_{0.37})_{20}(NbS_2)_{23}$. (Although the measured c lattice constant is closer to those of the 1Q′/25H and 2Q′/24H compounds, they are inadequate because there is no Nb content in a Q′ layer in contradiction to the XPS results.) To compare with the XRD pattern of sample 3, theoretical calculations are carried out for superlattices consisting of forty slabs of $Ni_{0.33}NbS_2$ in two cases that (1) each of three isolated

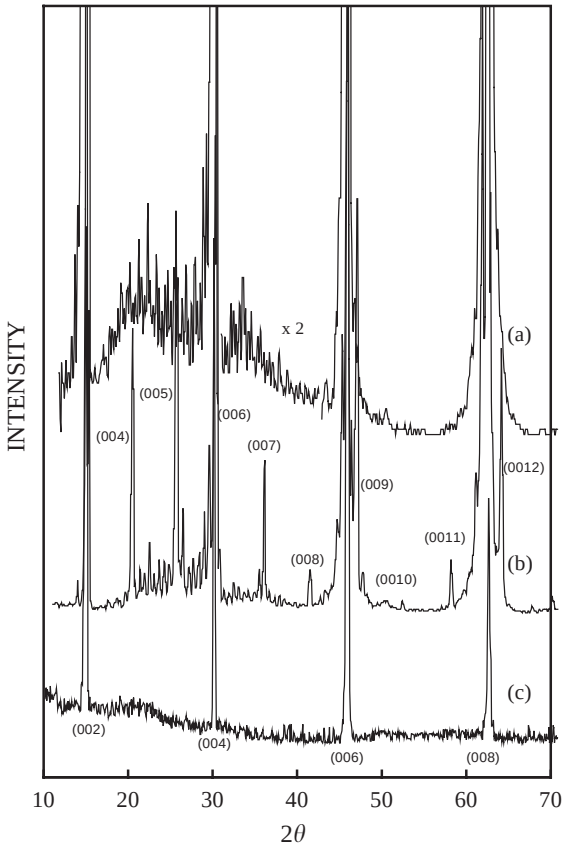

Fig. 2. XRD patterns of (a) sample 3, (b) sample 4, and (c) Ni_zNbS_2.

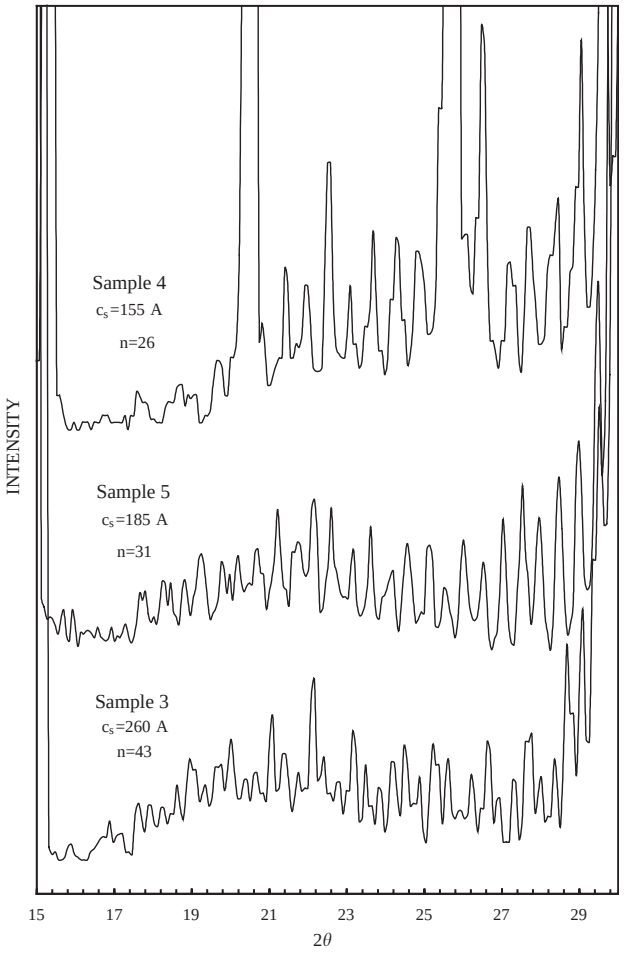

Fig. 3. Fine diffraction lines which arise from superlattices. c_s is a repeat distance along the c-axis and n is the number of layers per unit cell.

Ni layers is substituted with a CeS layer and (2) a Ni layer is substituted with a triple CeS layer. Diffraction intensities are calculated from

$$|F(00l)^2| = \left| \sum_i \sum_j f_{ij} \exp\{2\pi i(lz_{ij}/c_s)\} \right|^2, \quad (1)$$

where f_{ij} is the atomic form factor of atom j on layer i. Calculated results are only weakly dependent on the number of inserted CeS layers. It is found that a better agreement is attained in the former case. In the latter case the XRD pattern shows a clear envelope in contrast with the experiment result. Then we may suggest that Q′ layers are isolated in the superlattice (Fig. 4).

4. XPS results

Fig. 5 shows the Ce 3d XPS spectrum of the superlattice of the sample 5, which is compared with those of the 1Q′/3H compounds, $Ni_z(CeS)_{1.16}(NbS_2)_2$ and $(CeS)_{1.16}NbS_2$. It is well known that even only small Ni intercalation strengthens the bonding between two successive H layers in LTMDCs significantly. Then it is not surprising that strong Ce 3d lines are observed for the superlattices in spite of a small number of Q′ layers, because a cleavage happens preferentially at an interface between $Ce_xNb_{1-x-y}\square_yS$ and NbS_2 layers. The XPS spectrum of $(CeS)_{1.16}NbS_2$ has been discussed in a previous paper in detail [22], in which it has been suggested that the final state effect, which arises from the interconfiguration interaction in the presence of a core hole, plays a very important role. Despite the fact that Ce exists as a trivalent ion in $(CeS)_{1.16}NbS_2$, there are two peaks for each spin–orbit-split component. The main $3d_{5/2}$ and $3d_{3/2}$ peaks, which are located at 885 and 904 eV, respectively, are attributed to the poorly screened $3d^9f^2v^m(f^1)$ final state, where v^m is valence electrons. Shoulders at 4.0 eV below the main peaks are assigned to the well-screened $3d^9f^2v^{m-1}(f^2)$ final state. Because of the final state effect, it is difficult to determine the number of 4f electrons accurately without the aid of calculations such as have been made by Gunnarsson and Schönhammer [23]. The detailed comparison of the theoretical calculations with experimental results has been made by Fuggle et al. for many Ce compounds [24]. They have found that the intensity of the f^2 peak relative to the f^1 peak strongly depends not only on the probability of having two electrons in the ground state ($P(f^2)$), but also on the charge transfer energy (Δ) which is a measure of hybridization of f states with valence electrons. In typical trivalent compounds $P(f^2)$ is less than 0.05, although it has a great influence on the f^2 peak. In a strong hybridization system the XPS spectrum exhibits a larger f^2 peak comparable with a f^1 peak. For $(CeS)_{1.16}NbS_2$ Δ is about 0.1 eV, which gives an intermediate coupling strength nearly equal to that of Ce_3Pd_5 [22]. In Fig. 5 the f^2 peak of the sample 5 is larger than $(CeS)_{1.16}NbS_2$ and the spectrum rather resembles that of the 1Q′/3H compound. This fact indicates that the superlattice contains a $Ce_xNb_{1-x-y}\square_yS$ layer rather than that of a CeS layer. Longer Ce–S distances in the Q′ layer reduce hybridization of 4f electrons. Then if $P(f^2)$ remains unchanged, we may expect that the f^2 peak is reduced in intensity in contrast with the experimental result. At present the valence of Ce in a solid is usually treated as 3+ or 4+, because Ce^{2+} is has much higher energy than Ce^{3+} and Ce^{4+} and coupling of the states is much smaller than the f^1-f^2 energy separation. However, we may suggest that the valence of Ce in the Q′ layer is less than 3+. This conclusion is partially supported by increased Ce–S distances. Finally, a large number of Nb atoms affect the valence and bonding of Ce in the Q′ layer significantly.

In contrast with the XRF result, Ni 2p spectra show no evidence for Ni intercalation except for the sample 1

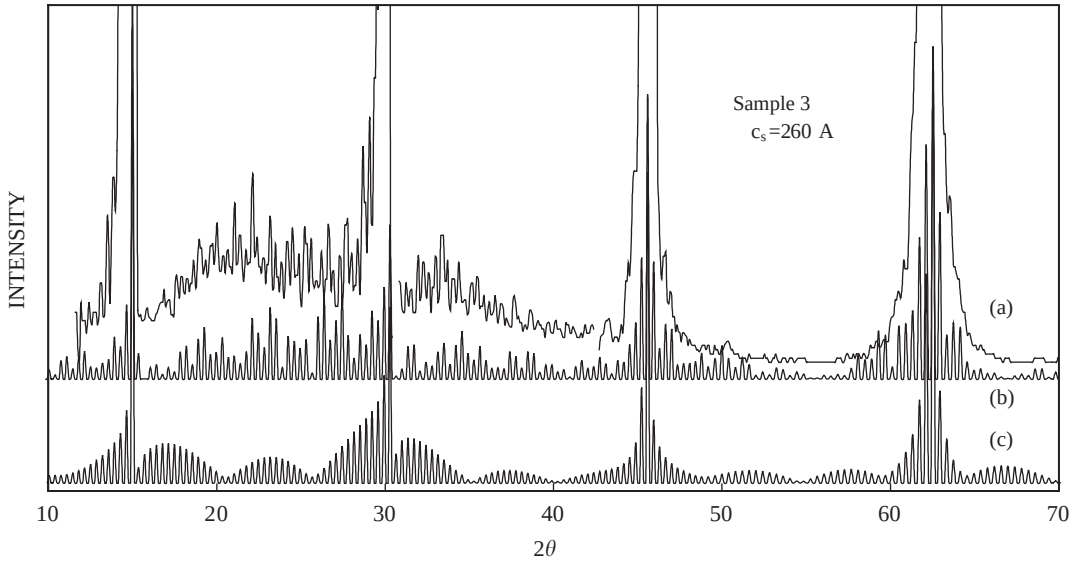

Fig. 4. Comparison of the measured XRD pattern of the sample 3 with calculation results. (a) Experimental result. (b) and (c) Calculation results, which are obtained for supercells consisting of 43 layers. Stacking sequences are (b) HHHHHHHHQHHHHHHHHHHHHQHHHHHHHHHHHHHHQHHHHHHHH and (c) QQQHHHHHH···HHHH, respectively.

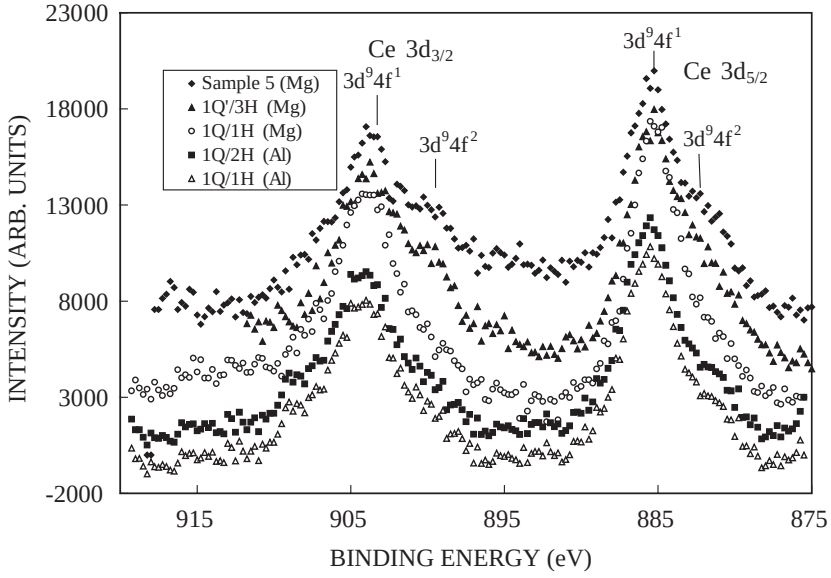

Fig. 5. Ce 3*d* XPS spectra. 1Q/1H and 1Q/2H compounds are $(CeS)_{1.16}NbS_2$ and $Ni_z(CeS)_{1.16}(NbS_2)_2$, respectively.

(see Fig. 6). This is due to high-surface sensitivity of the XPS technique. If the top surface layer consists of a Q′ layer, Ni is located underneath a $Ce_xNb_{1-x-y}\square_yS$ and a NbS_2 layer. Then the mean free path of electrons of about 17 Å is required to detect the element because the entrance slit of the CMA is located in a direction tilted by 42.5° with respect to the normal surface. However, the mean free path for Ni 2*p* photoelectrons is about 10 Å at the kinetic energy of 400 eV. Consequently, a large part of them cannot arrive at the CMA. The XRF and the STM results discussed later show that the superlattices as well as the 1Q′/3H and 1Q′/4H compounds contain Ni in a crystal, which is localized as a divalent ion at van der Waals gaps between two successive NbS_2 layers [25,26].

Fig. 7 shows Nb 3*d* and S 2*s* XPS spectra. The Nb 3*d* spectra of $(SmS)_{1.19}NbS_2$ and $(BiS)_{1+x}NbS_2$ reveal two spin–orbit-split peaks which are separated by 2.4 eV. Their intensity ratio is nearly equal to the statistical value of the core levels, that is 3:2. It is found that for

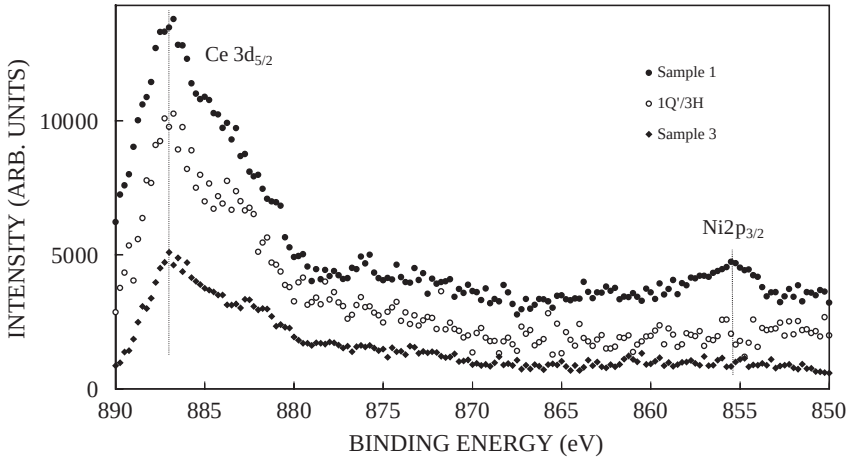

Fig. 6. Ni 2*p* XPS spectra.

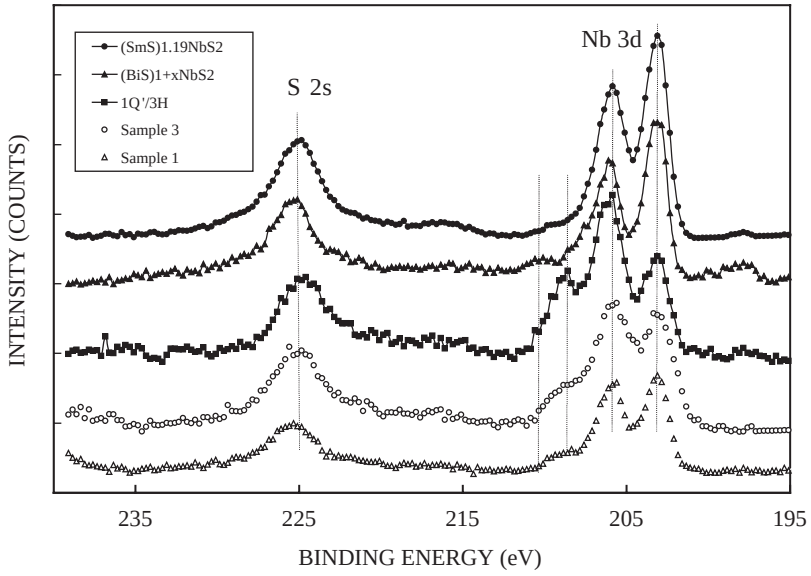

Fig. 7. Nb 3*d* XPS spectra, which are accompanied with S 2*s* structures on the higher binding energy side.

the samples containing the Q′ layer, peak intensities are deviated largely from the statistical value and an additional peak appears on the higher binding energy side. This deviation becomes more prominent with the density of the Q′ layers. Then it is reasonable to relate the deviation and the appearance of the new peak to Nb in the Q′ layer. The new peak may be assigned to Nb $3d_{3/2}$ levels in $Ce_xNb_{1-x-y}\square_yS$ layers. Then it is suggested that Nb in the Q′ layer is in a higher oxidation state than that in the H layer and the chemical shift is about 3.3 eV. A small peak is found at 210 eV for $(BiS)_{1+x}NbS_2$. This peak may be attributed to oxidized Nb at a surface. Taking the three different Nb sites into account, the XPS spectrum of the 1Q′/3H compound is decomposed into three pairs of Lorenzian peaks as shown in Fig. 8. Here it is noted that the intensity of an Nb2 peak is comparable with an Nb1 peak in spite of a smaller concentration. This fact implies that the top surface layer consists of a Q′ layer.

5. STM results

Fig. 9 shows the STM image of the sample 5 and its height profiles along the [01] and [21] directions. The image reveals hexagonal arrays of bright spots, reflecting the surface electronic structure of the H layer. In the image brighter spots are observed. They form a hexagonal $\sqrt{3}a_0 \times \sqrt{3}a_0$ supercell in the (a,b)-plane, where a_0 is the interatomic distance of the top S layer. The same supercell happens in the Ni intercalation derivative of NbS_2 at Ni concentration of 1/3 [27]. Fig. 10 shows the crystal structure, in which Ni atoms occupy a third of octahedral sites in van der Waals gaps,

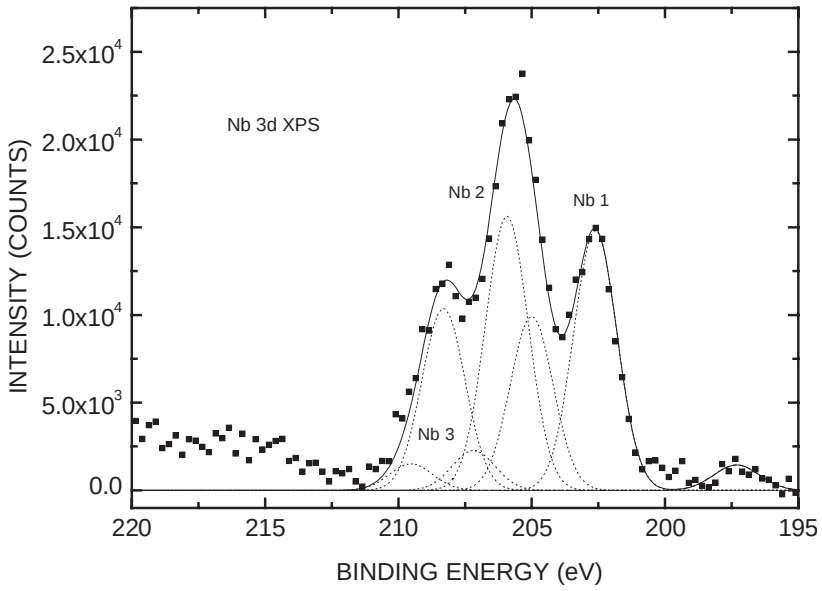

Fig. 8. Nb 3*d* XPS spectrum of the 1Q′/3H compound after decomposing with Lorentzian curves of $3d_{5/2}$ and $3d_{3/2}$ peaks. Nb1 and Nb2 represent Nb in the H and Q′ layers, respectively, and Nb3 represents oxidized Nb at a surface.

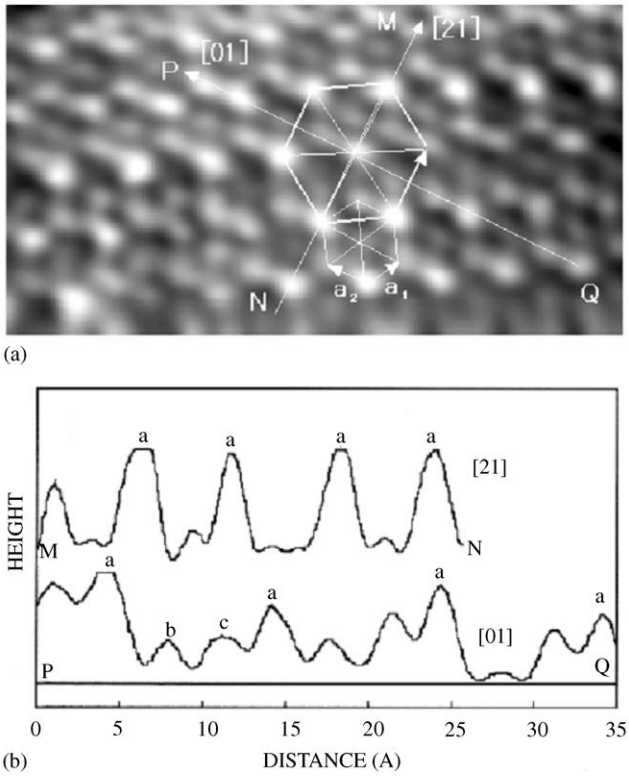

Fig. 9. STM image and height profiles of the sample 3. (a) STM image reveals brighter spots in a hexagonal structure. A supercell image is rotated by 30° with respect to the unit cell of NbS_2, in which $\vec{a}_1$ and $\vec{a}_2$ are the fundamental translation vectors of the top S layer. (b) Height profiles in the [21] and [01] directions.

located just above and below Nb sites and the $\sqrt{3}a_0 + \sqrt{3}a_0$ supercell is rotated by 30° with respect to the hexagonal unit cell of the top S layer. Till now no STM

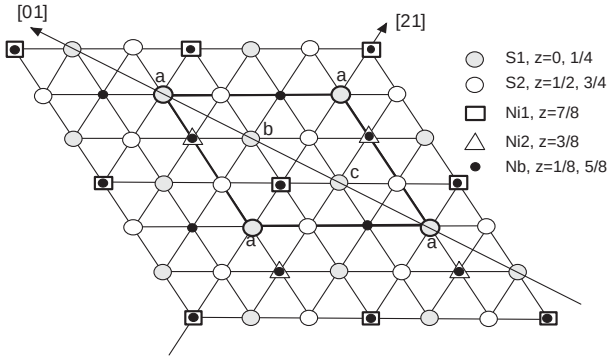

Fig. 10. Crystal structure for $Ni_{0.33}NbS_2$.

studies have been made for $Ni_{1/3}NbS_2$ as far as the present authors know. For $M_{1/3}NbS_2$ (M = Fe and Co) a $\sqrt{3}a_0 + \sqrt{3}a_0$ structure have been observed by Prodan et al. [28]. They have suggested from a comparison with calculation results based on the extended Hûckel tight binding (EHTB) approximation that the supercell images are formed by charge redistribution on a surface, which is induced by charge transfer from Ni intercalates. According to their results, a part of surplus charge is located on one S atom (the *a* site in Fig. 10) and a part is shared between two remaining S atoms at the *b* and *c* sites. The height profiles in Fig. 10(b) support their calculation results. A saddle point appears between two brighter spots in the [21] direction and three different maxima appear at S positions in the [01] direction. The STM image shows that Ni uptake is close to 1/3 and charge redistribution happens on the H layer.

The supercell image could not be obtained at bias voltage less than 0.3 V. This result totally contrasts with

the STM observations of the 1Q/1H compounds and 2H-NbS_2. For the latter compounds bright spots are imaged at bias voltage less than 0.1 eV obviously. This fact indicates that a metal–semiconductor transition happens in the H layers. Alternatively speaking, the energy bands are opened at the Fermi level. According to the band calculation of Fong and Cohen [29], the Fermi surface of 2H-$NbSe_2$ akin to 2H-NbS_2 consists of a cylindrical hole pocket along the K–H direction and a spherical hole pocket at the A point. In $Ni_{1/3}NbS_2$ a new Brillouin zone appears in forming a $\sqrt{3}a_0 + \sqrt{3}a_0$ supercell. Its volume is smaller than that of the Brillouin zone of 2H-NbS_2 by a factor of 3. After reconstruction of energy bands, a new Brillouin zone has a cylindrical hole pocket at the Γ point. It can be collapsed by charge transfer from intercalates. In the present case the Brillouin zone is furthermore sliced into thinner hexagonal plates by formation of a superlattice in a direction perpendicular to the layers. If all unoccupied energy states of the lowest conduction band are filled with additional electrons, then hole pockets might collapse completely.

No STM images are obtained for the Q′ layer. This situation resembles that of the Q layers of 1Q/1H misfit-layer compounds. For the latter compounds only the H layers are imaged although both layers appear at the same probability by a cleavage. It remains mysterious for a long time. Recently it has been suggested by one of the present authors that layer thickness plays an important role on the STM observations [30]. If the top surface layer consists of a very thin layer with semiconducting properties, electrons tunneling from the metallic NbS_2 layer underneath, pass through the semiconducting energy gap of the top surface layer as if it is transparent for tunneling phenomenon. This is comparable to Al_2O_3 in the metal–Al_2O_3–Al tunneling junction. In other words, a single Q or Q′ layer is thin enough for electrons to tunnel from the NbS_2 layer underneath, while there are negligible tunneling electrons from a Q or Q′ layer at small bias voltage. A double Q layer in $(Pb_{1-x}Sb_xS)_{2.28}NbS_2$, on the other hand, allows the STM observation of tetragonal arrays of bright spots which are peculiar to a Q layer. This result means that a double Q layer is thick enough to prevent electrons from tunneling from the NbS_2 layer underneath. Then no STM observations of the Q′ layer imply that they are inserted as a single layer in superlattices, in consistency with the XRD result.

6. Conclusions

The new misfit-layer compounds of the 1Q′/3H and 1Q′/4H types of structure are prepared by chemical-vapor transport reaction in a closed silica ampoule. They are constructed by alternately stacking of a $Ce_xNb_{1-x-y}\square_yS$ layer and a $(Ni_z)_{n-m}(NbS_2)_n$ layer ($m = 1$; $n = 3, 4$). The oxidation state of Ce is smaller than 3+ and the thickness of a $Ce_xNb_{1-x-y}\square_yS$ layer is larger by about 1.0 Å than that of a CeS layer. The natural superlattices of $(Ce_xNb_{1-x-y}\square_yS)_m(Ni_z)_{n-m}(NbS_2)_n$ ($n > 10$) are found from the same ampoule. The crystal structures of the 1Q′/3H and 1Q′/4H compounds and the natural superlattice of the 3Q′/23H type are illustrated in Fig. 11. The superlattice is formed by substituting some Ni layers in Ni_zNbS_2 with a Q′ layer. From a different point of view they are regarded as long period polytypes consisting of $Ce_xNb_{1-x-y}\square_yS$ and $(Ni_z)_{n-m}(NbS_2)_n$ layers. Since interlayer interaction is very small in layer compounds,

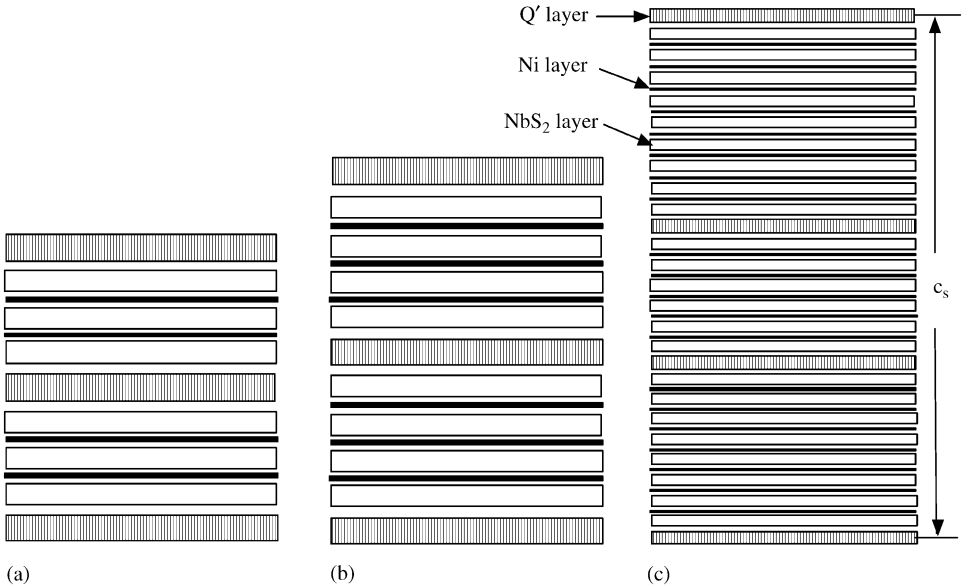

Fig. 11. Schematic diagrams for crystal structures of (a) 1Q′/3H compound, (b) 1Q′/4H compound and (c) superlattice of the 3Q′/23H type.

there are many polytypes and morphologies. In fact the short-period polytypes of 1T, 2H, 3R, 4H and 6R are found in LTMDCs. A long period polytype has been found for $Tl_2Ba_2Ca_nCu_{1+n}O_{6+2n}$, one of the layered high-temperature superconductors [31]. It contains two perovskite blocks of $n = 3$ and 4 and double and single TlO layers in a unit cell and the c lattice constant is about 210 Å. Then it is not surprising that a long period polytype happens for misfit-layer compounds. If it is formed with 1Q′/3H (3) and 1Q′/4H (4) slabs, the stacking sequences of 434333 ($n = 26$), 4343343 ($n = 31$) and 4334333433 ($n = 43$) result in the large periods of about 158, 188 and 261 Å, respectively.

The H layers of some of the superlattices behave as a narrow-gap semiconductor. Atomically ordered images are obtained at a bias voltage from 0.3 to 0.7 eV. They reveal a $\sqrt{3}a_0 + \sqrt{3}a_0$ superlattice in the (a, b)-plane. Then we may consider that the folding of energy bands happens along the direction perpendicular to layers and in the (k_x, k_y)-plane, and the resulting Brillouin zone is very small with a thin hexagonal plate-like shape. The XPS result shows that Nb in the Q′ layers is in a higher oxidation state than that in the H layers. If it exists as a trivalent ion suggested by Roesky et al. [29] and Moëlo et al. [32], transferred electrons might be smaller than those from a CeS layer owing to atomic deficits at a metal site. If the oxidation state is 4+, transferred electrons are comparable with those of the Q layer. In both cases, however, the d_{z^2} band, the lowest conduction band of the NbS_2 layer would be filled incompletely with electrons. Then we may conclude that the metal–semiconductor transition results from the folding of energy bands by periodic potentials along the c-axis and in the (a, b)-plane.

Acknowledgments

The authors thank Mr. H. Honma and Mr. Y. Komata and the staff of Rigaku International Cooperation for XRF analyses.

References

[1] L. Otero-Diaz, J.D. Fitz Gerald, T.B. Williams, B.G. Hyde, Acta Crystallogr. 41 (1985) 405.
[2] A. Meerschaut (Ed.), Incommensurate Sandwiched Layered Compounds, Mater. Sci. Forum, Vols. 100 & 101, Trans Tech Pub., Switzerland, 1992.
[3] G.A. Wiegers, Prog. Soid State Chem. 24 (1996) 1.
[4] J. Brandt, J. Kanzow, K. Roβnagel, L. Kipp, M. Skibowski, E.E. Krasovskii, W. Schattke, M. Traving, J. Stettner, W. Press, C. Dieker, W. Jäger, J. Electron Spectosc. Relat. Phenom. 555 (2001) 114–116.
[5] J. Brandt, L. Kipp, M. Skibowski, E.E. Krasovskii, W. Schattke, E. Spiecker, C. Dieker, W. Jäger, Surf. Sci. 705 (2003) 532–535.
[6] E.E. Krasovskii, O. Tiedje, W. Schattke, J. Brandt, J. Kanzow, K. Roßnagel, L. Kipp, M. Skibowski, M. Hytha, B. Winkler, J. Electron Spectrosc. Relat. Phenom. 1133 (2001) 114–116.
[7] C. Umrigar, D.E. Ellis, D. Wang, H. Krkauer, M. Posternak, Phys. Rev. B 26 (1982) 4935.
[8] H.E. Brauer, H.I. Starnberg, L.J. Holleboom, H.P. Hughes, V.N. Strocov, J. Phys.: Condens. Matter 11 (1999) 8957.
[9] Y. Ohno, Phys. Rev. B 44 (1991) 1281.
[10] Y. Ohno, J. Phys.: Condens. Matter 6 (1994) 8655.
[11] C.M. Fang, A.R.H.F. Ettema, C. Haas, G.A. Wiegers, Phys. Rev. B 52 (1995) 2336.
[12] A. Lafond, A. Nader, Y. Moëlo, A. Meerschaut, A. Briggs, S. Perrn, P. Monceau, J. Rouxel, J. Alloys Compds. 261 (1997) 114.
[13] A. Cario, A. Lafond, P. Palvadeau, C. Deudon, A. Meerschaut, J. Solid State Chem. 145 (1999) 58.
[14] C. Deudon, A. Lafond, O. Leynaud, Y. Moëlo, A. Meerschaut, J. Solid State Chem. 155 (2000) 1.
[15] T. Terashima, N. Kojima, H. Kitagawa, H. Okamoto, t. Mitani, J. Phys. Soc. Jpn. 62 (1993) 2166.
[16] J.E. Fischer, in: F. Lévy (Ed.), Physics and Chemistry of Materials with Layered Structures, Vol. 6, Reidel Pub. Comp., Dordrecht, 1979, p. 481.
[17] R.E. Camley, D.L. Mills, Phys. Rev. B 29 (1984) 1695.
[18] Y. Ohno, T. Urata, unpublished.
[19] T. Rouxel, A.Le. Blanc, A. Royer, Bull Soc. Chim. Fr. 6 (1971) 2019.
[20] R. Roesky, A. Meerschaut, A. van der Lee, J. Rouxel, Mater. Res. Bull. 29 (1994) 1149.
[21] A. Meerschaut, T. David, Y. Moëlo, J. Rouxel, Eur. J. Solid State Inorg. Chem. 33 (1996) 551.
[22] Y. Ohno, Phys. Rev. B 48 (1993) 5515.
[23] O. Gunnarsson, K. Schrönhammer, Phys. Rev. B 27 (1983) 7330.
[24] J.C. Fuggle, F.U. Hillebrecht, Z. Zołnierek, R. Lässer, Ch. Freiburg, O. Gunnarsson, K. Schrönhammer, Phys. Rev. B 27 (1983) 7330.
[25] R.H. Friend, A.R. Beal, A.D. Yoffe, Philos. Mag. 35 (1977) 1269.
[26] A.R. Beal, W.Y. Liang, Philos. Mag. 33 (1976) 121.
[27] W.B. Clark, J. Phys. C 9 (1976) L693.
[28] A. Prodan, V. Marinković, M. Rojsek, N. Jug, H.J.P. van Midden, F.W. Boswell, J.C. Bennett, H. Böhn, Sur. Sci. 476 (2001) 71.
[29] C.Y. Fong, M.L. Cohen, Phys. Rev. Lett. 32 (1974) 720.
[30] Y. Ohno, T. Wada, J. Phys. Soc. Jpn. 70 (2001) 2082.
[31] G. Van Tendeloo, S. Amelinckx, in: A. Meerschaut (Ed.), Mater. Sci. Forum, Vols. 100 & 101, Trans Tech Pub., Switzerland, 1992, p. 327.
[32] Y. Moëlo, A. Meerschaut, J. Rouxel, C. Auriel, Chem. Mater. 7 (1995) 1759.